MEASUREMENTS OF MULTIJET EVENT SHAPES AND PHOTON PRODUCTION WITH THE ATLAS DETECTOR* **

L. Carminati

on behalf of the ATLAS Collaboration

Università degli Studi and INFN Milano, Italy

Received 1 February 2023, accepted 7 February 2023, published online 25 May 2023

The study of jets and photons production in proton–proton (pp) collisions is a fundamental part of the ATLAS experimental physics program. In this contribution, measurements of new event-shape jet observables and inclusive isolated-photon production using LHC pp collision data at $\sqrt{s} = 13$ TeV with the ATLAS detector will be discussed. The results are unfolded for detector effects and compared to the state-of-the-art theoretical predictions.

DOI:10.5506/APhysPolBSupp.16.5-A1

1. Introduction

Measurements of multijet event shapes and prompt photon production with the ATLAS detector [1] at the LHC are important for several reasons. On the one hand, they constitute a fundamental test of perturbative QCD behaviour at hadron colliders. On the other hand, they are crucial in tuning Monte Carlo (MC) event generators and to identify new discriminating variables in the search for physics beyond the Standard Model (SM). In this contribution, two recent measurements on multijet event shapes [2] and inclusive prompt photon production [3] will be briefly presented.

2. Multijet event shapes using optimal transport

Event shapes are a family of observables used to describe the flow of energy in collider events. A novel class of observables that quantifies the

* Presented at the Diffraction and Low-x 2022 Workshop, Corigliano Calabro, Italy, 24–30 September, 2022.

** Copyright 2022 CERN for the benefit of the ATLAS Collaboration. CC-BY-4.0 license.

isotropy of collider events was recently proposed [4]. These observables measure how 'far' a collision event is from a symmetric radiation reference pattern (U_N) using the Energy-Mover's Distance (EMD) framed in terms of the optimal transport problem [5]. The EMD is defined as the minimum amount of work necessary to transport one event E with M particles into another event E' of equal energy with M' particles by movements of energy f_{ij} from particle i in one event to particle j in the other. In this contribution, the results for two event shape observables are reported: the EMD from a quasi-uniform ring-like geometry with $N = 128$ points (I^{128}_{Ring}), and the special case of $N = 2$ points (I^{2}_{Ring}). The reference geometries are shown in Fig. 1.

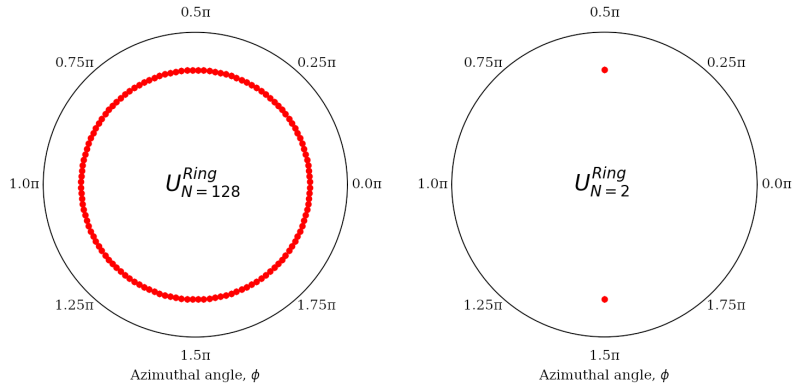


Fig. 1. Reference geometries with ring-like symmetry with (left) $N = 128$ and (right) $N = 2$ points [2].

All observables are presented following the historical convention that the least isotropic ('dijet-like') topology is near values of zero, and the most isotropic topology is near values of one. Therefore, the results of this measurement are presented in terms of I^{2}_{Ring} and 1-I^{128}_{Ring}.

The analysis is based on data from the Run 2 LHC pp collisions at $\sqrt{s} = 13$ TeV recorded by the ATLAS detector for a total integrated luminosity of 139 fb^{-1}. PYTHIA is used as the nominal MC generator for unfolding. In addition, two sets of Sherpa dijet events are considered with the default AHADIC or the Lund cluster hadronisation model. Two sets of Herwig multijet events are generated using either the default angle-ordered or alternative dipole parton shower (PS). Finally, two samples of dijet events are produced at NLO with Powheg Box V2, matched to either the PYTHIA 8 or angle-ordered Herwig 7 PS. All simulated events are produced using a full detector simulation and superimposed with the simulated minimum-bias interactions to represent pile-up interactions.

Events are required to have at least two selected jets ($N_{\text{jet}} \geq 2$) and to satisfy $H_{\text{T2}} \geq 400$ GeV, where H_{T2} is the scalar sum of the leading and sub-leading jet transverse momenta. The distributions of 1-I^{128}_{Ring} and I^{2}_{Ring} in events with $N_{\text{jet}} \geq 2$ and $H_{\text{T2}} \geq 500$ GeV are shown in Fig. 2. More distributions can be found in Ref. [2].

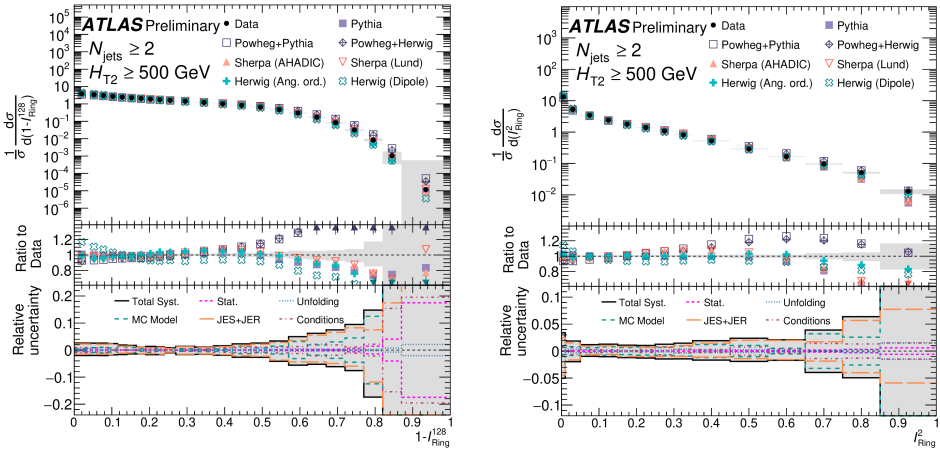


Fig. 2. The unfolded 1-I^{128}_{Ring} (left) and I^{2}_{Ring}(right) distributions in data (closed circles) compared to predictions from several MC generators [2]. The middle panel displays the ratios of different event generator predictions to the unfolded data. Event generator predictions are displayed as different marker styles. The grey band in the upper and middle panels indicates the total uncertainty of the measurement. The lower panel summarises the various sources of systematic uncertainties on the measurement. The total uncertainty is shown as a solid black line.

The agreement between the unfolded data and the simulated events tends to be the best in balanced, dijet-like arrangements and deteriorates in more isotropic configurations. For the measurement of I^{2}_{Ring}, the predictions of NLO MCs generally outperform those of LO simulation. In the measurement of 1-I^{128}_{Ring}, no single event generator accurately describes the distribution. In particular, the descriptions of the NLO Powheg+PYTHIA and Herwig simulations differ in the region sensitive to isotropic configurations. For both event shapes, no differences are notable between the Sherpa hadronisation models.

3. Measurement of inclusive isolated-photon production

Prompt photon production provides a more powerful testing ground for perturbative QCD in a cleaner environment than dijet production since it is less affected by hadronisation effects. In particular, it can be used in

the global QCD fits to constrain the gluon parton distribution functions. The production of high-p_{T} prompt-photons proceeds at LO via two mechanisms: direct processes and fragmentation processes. The fragmentation contribution is typically cumbersome to calculate and relies on fragmentation functions that must be determined from comparisons with data. The main background to prompt-photon production comes from high transverse momentum π^0 produced in jets fragmentation and misidentified as photons.

The measurements presented in this contribution rely on full Run 2 dataset ($L = 139$ fb^{-1}) collected by the ATLAS detector. The event selection proceeds as follows: at least one photon with transverse energy $E_{\mathrm{T}}^{\gamma} > 250$ GeV and $|\eta^{\gamma}| < 2.37$, excluding the $1.37 < |\eta^{\gamma}| < 1.56$ region, is required. Tight photon identification requirements are applied to the selected photon candidates. Finally, to reduce the background from jets and the fragmentation contributions, an isolation criterium is used, requiring the transverse energy in a cone of radius $R = 0.2$ or 0.4 around the photon direction to be less than $4.2 \times 10^{-3} E_{\mathrm{T}}^{\gamma} + 4.8$ GeV after subtraction of the transverse energy of the photon candidate itself. The measured purity of the selected sample is found to be greater than 95%.

Data are unfolded at the particle level using a bin-by-bin method. The measurements of inclusive isolated-photon production cross sections as functions of E_{T}^{γ} in six bins of η^{γ} with two different isolation cone radii are shown in Fig. 3. The data are compared with the predictions at NLO computed using the programs Jetphox 1.3.1-2 and Sherpa 2.2.2. The state-of-the-art NNLO QCD predictions are calculated in the NNLOJET framework. The measurement uncertainty is dominated by systematics up to approximately 1 TeV. For both cone radii, the NNLO predictions (including direct- and fragmentation-photon components) give a good description of the data within the uncertainties, except in the region of $1.56 < \eta^{\gamma} < 1.81$, where the calculations underestimate the data.

Ratios of differential cross sections with different cone radii allow to investigate very precisely the handling of the fragmentation contribution by the theoretical calculations: most of the theoretical and experimental uncertainties cancel out in the ratio leading to a precision on the percent level as shown in Fig. 4: generally, a good agreement is observed between data and theoretical calculations [3].

4. Conclusions

Two new interesting measurements released by the ATLAS Collaboration have been discussed. Event shape observables are shown to be capable of exposing a remote region of the QCD phase space that is difficult to model and is relevant to many searches for physics beyond the SM. In addition, new

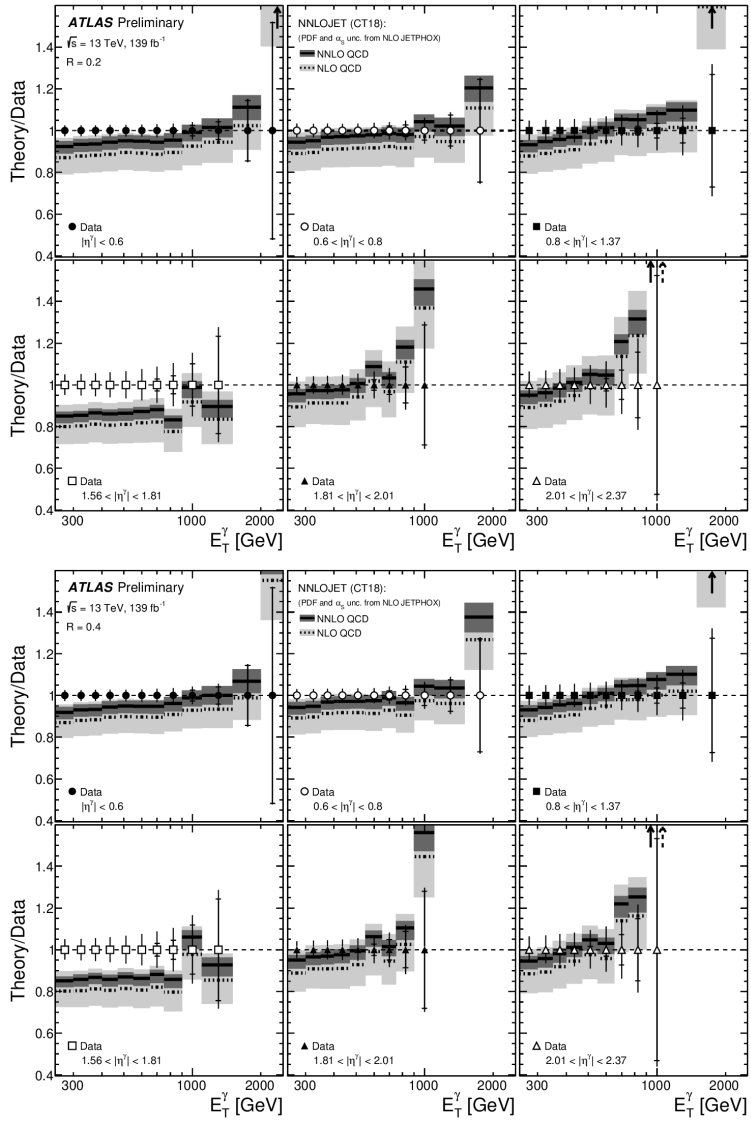


Fig. 3. Ratio of the NLO (dotted lines) and NNLO (solid lines) QCD calculations from NNLOJET and the measured differential cross sections for isolated-photon production with $R = 0.2$ (top) and $R = 0.4$ (bottom) as functions of E_{T}^{γ} in six regions of η^{γ} [3]. The inner (outer) error bars represent the statistical uncertainties (statistical and systematic uncertainties added in quadrature). The shaded bands represent the theoretical uncertainties.

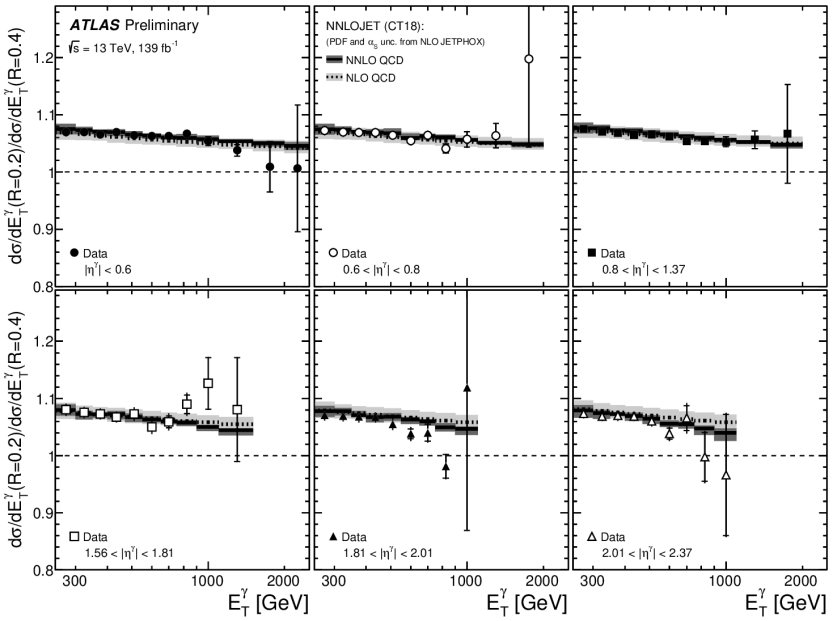


Fig. 4. Measured ratios of the differential cross sections for inclusive isolated-photon production for $R = 0.2$ and $R = 0.4$ as functions of E_{T}^{γ} in different η^{γ} regions [3]. The NLO (dotted lines) and NNLO (solid lines) QCD predictions from NNLOJET are also shown. The inner (outer) error bars represent the statistical uncertainties (statistical and systematic uncertainties added in quadrature) and the shaded bands represent the theoretical uncertainties.

measurements of inclusive isolated-photon cross sections and ratios of cross sections with different isolation cone radii have been presented reporting a good agreement with the state-of-the-art theoretical predictions.

REFERENCES

[1] ATLAS Collaboration, *J. Instrum.* **3**, S08003 (2008).

[2] ATLAS Collaboration, Technical report ATLAS-CONF-2022-056, CERN, Geneva, 2022, https://cds.cern.ch/record/2824758

[3] ATLAS Collaboration, Technical report ATLAS-CONF-2022-065, CERN, Geneva, 2022, https://cds.cern.ch/record/2835957

[4] C. Cesarotti, J. Thaler, arXiv:2004.06125 [hep-ph].

[5] P.T. Komiske, E.M. Metodiev, J. Thaler, *Phys. Rev. Lett.* **123**, 041801 (2019).